

# Surface anisotropy, hysteretic, and magnetic properties of magnetite nanoparticles: A simulation study

J. Mazo-Zuluaga, J. Restrepo, F. Muñoz, and J. Mejía-López

Citation: *Journal of Applied Physics* **105**, 123907 (2009); doi: 10.1063/1.3148865

View online: <https://doi.org/10.1063/1.3148865>

View Table of Contents: <http://aip.scitation.org/toc/jap/105/12>

Published by the [American Institute of Physics](#)

---

## Articles you may be interested in

[Static and dynamic magnetic properties of spherical magnetite nanoparticles](#)

*Journal of Applied Physics* **94**, 3520 (2003); 10.1063/1.1599959

[Effect of surface anisotropy on the magnetic properties of magnetite nanoparticles: A Heisenberg–Monte Carlo study](#)

*Journal of Applied Physics* **103**, 113906 (2008); 10.1063/1.2937240

[Adsorption of biomedical coating molecules, amino acids, and short peptides on magnetite \(110\)](#)

*The Journal of Chemical Physics* **143**, 044705 (2015); 10.1063/1.4927327

[Low frequency hysteresis loops of superparamagnetic nanoparticles with uniaxial anisotropy](#)

*Journal of Applied Physics* **107**, 123909 (2010); 10.1063/1.3445879

[Simple models for dynamic hysteresis loop calculations of magnetic single-domain nanoparticles: Application to magnetic hyperthermia optimization](#)

*Journal of Applied Physics* **109**, 083921 (2011); 10.1063/1.3551582

[Spin disorder and magnetic anisotropy in  \$\text{Fe}\_3\text{O}\_4\$  nanoparticles](#)

*Journal of Applied Physics* **99**, 083908 (2006); 10.1063/1.2191471

---

**AIP** | Journal of Applied Physics SPECIAL TOPICS



# Surface anisotropy, hysteretic, and magnetic properties of magnetite nanoparticles: A simulation study

J. Mazo-Zuluaga,<sup>1,a)</sup> J. Restrepo,<sup>1</sup> F. Muñoz,<sup>2</sup> and J. Mejía-López<sup>2</sup>

<sup>1</sup>*Grupo de Estado Sólido, Grupo de Instrumentación Científica y Microelectrónica, Instituto de Física, Universidad de Antioquia, A.A. 1226, Medellín, Colombia*

<sup>2</sup>*Facultad de Física, Pontificia Universidad Católica, Av. Vicuña Mackenna 4860, Santiago, Chile*

(Received 5 March 2009; accepted 10 May 2009; published online 17 June 2009)

In this study we address the role of surface anisotropy on the hysteretic properties of magnetite  $\text{Fe}_3\text{O}_4$  nanoparticles and the circumstances yielding both horizontal and vertical shifts in the hysteresis loops. Our analysis involves temperature dependence and particle size effects. Different particle sizes ranging from 2 up to 7 nm were considered. Our theoretical framework is based on a three-dimensional classical Heisenberg model with nearest magnetic neighbor interactions involving tetrahedral (*A*) and octahedral (*B*) irons. Cubic magnetocrystalline anisotropy for core spins, single-ion site anisotropy for surface spins, and interaction with a uniform external magnetic field were considered. Our results revealed the onset of low temperature exchange bias field, which can be positive or negative at high enough values of the surface anisotropy constant ( $K_S$ ). Susceptibility data, computed separately for the core and the surface, suggest differences in the hard-soft magnetic character at the core-surface interface. Such differences are  $K_S$ -driven and depend on the system size. Such a hard-soft interplay, via the surface anisotropy, is the proposed mechanism for explaining the observed exchange bias phenomenology. Our results indicate also that the strongly pinned spins at high enough surface anisotropy values are responsible for both the horizontal and vertical shifts in the hysteresis loops. The dependences of the switching and exchange bias fields with the surface anisotropy and temperature are finally discussed. © 2009 American Institute of Physics.

[DOI: [10.1063/1.3148865](https://doi.org/10.1063/1.3148865)]

## I. INTRODUCTION

Since the exchange bias was discovered in 1956 by Meiklejohn and Bean,<sup>1</sup> most of the reported work on literature has been devoted to the study of layered antiferromagnetic (AFM)-ferromagnetic (FM) systems, including mainly, thin films and small particles.<sup>2,3</sup> Exchange bias has also been observed in interfaces involving the presence of a ferrimagnet (ferri)like AFM-ferri (Ref. 4) and FM-ferri (Ref. 5) systems. However, despite the fact that fine particles were the first type of system where exchange bias was observed, most of the related work on particles deals with those consisting of a FM core surrounded by its respective AFM or ferrimagnetic native oxide,<sup>6–10</sup> and some very few studies on pure systems exhibiting exchange bias, e.g., pure ferri or AFM nanoparticles, have been carried out.<sup>11,12</sup> In the case for instance of AFM NiO nanoparticles with average size ranging from 5 to 80 nm, large coercivities and shifted hysteresis loops were reported for all samples after field cooling.<sup>11</sup> Numerical modeling was also performed in order to endorse the occurrence of multisublattice spin configurations instead of a two-sublattice model. The model was based on considerations of low coordination at surface sites and weak coupling between sublattices, allowing a variety of reversal paths for the spins upon cycling the applied field as a mechanism for exchange bias. Experimental evidence and numerical calculations for organic-coated  $\text{NiFe}_2\text{O}_4$  nanoparticles have also

demonstrated the occurrence of shifted hysteresis loops after field cooling, consistent with a model of ferrimagnetically aligned core spins and a spin-glasslike surface layer.<sup>12,13</sup> Here, nanoparticles were obtained by grinding high purity  $\text{NiFe}_2\text{O}_4$  powders in kerosene and oleic acid. Such organic surfactant was found to be strongly bonded to the surface of the nanoparticles. In this case, exchange bias behavior was associated to the existence of many surface canted spin states, one of which is selected by field cooling, separated by energy barriers (smaller than a certain freezing temperature) which can be overcome by thermal activation. An initial study on this kind of nanoparticles revealed an extremely strong spin pinning effect, presumably associated to surface cations bonded to the organic molecules.<sup>14</sup> The long-chain surfactant molecules coating the  $\text{NiFe}_2\text{O}_4$  particles are known to adsorb via the action of their polar terminal carboxyl group ( $-\text{COOH}$ ), which can result in an increase in surface anisotropy. Concerning pure ferrimagnetic magnetite nanoparticles, exchange bias and surface spin-glasslike behaviors have been reported to occur in  $\text{Fe}_3\text{O}_4$  nanoparticles compacted under high pressure.<sup>15</sup> In the field cooling process a preferred configuration is imposed upon the spin-glasslike surface spins. When the cooling field is removed, the ferrimagnetic core (with a higher ordering temperature) experiences the field generated by the frozen surface spins in the direction of the previously applied field, resulting in a shift in the hysteresis loop, i.e., the hysteresis loop offset arises from the exchange coupling between the spin-glasslike surface and core spins.<sup>15</sup> Another related ferrimagnetic oxide system,

<sup>a)</sup>Electronic addresses: [johanmazo@gmail.com](mailto:johanmazo@gmail.com) and [jomazo@fisica.udea.edu.co](mailto:jomazo@fisica.udea.edu.co).

namely,  $\gamma\text{-Fe}_2\text{O}_3$ , has also been widely studied from the point of view of hysteretic behavior and exchange bias properties.<sup>16–20</sup> Summarizing, those studies suggesting the occurrence of a “surface spin-glasslike state” are consistent with a surface spin disordered layer freezing below certain low temperature and behaving in an entirely different manner from the core. Such a spin-glasslike surface can be thought, in analogy with layered systems, as playing the role of an “AFM” layer surrounding a ferrimagnetic core. However, even though this intuitive picture can seem simple, a full understanding of the exchange bias properties of pure nanoparticles seems to be far beyond standard exchange bias models. Even though studies of bulk ferris with exchange bias behavior have not been systematically carried out, some examples can be found in the literature such as amorphous rare-earth based alloys<sup>21,22</sup> and some oxide type ferris.<sup>23,24</sup>

Magnetite nanoparticles possess some of the characteristics needed for the occurrence of shifted hysteresis loops. On the one hand, the presence of competing interactions can lead to magnetic frustration on the surface due to undercoordination. In magnetite, different superexchange integrals, namely,  $J_{AA} < 0$ ,  $J_{AB} < 0$  and  $J_{BB} > 0$ , are present. The inter-sublattice  $J_{AB}$  superexchange interaction, which is AFM, is dominant and it contributes to the appearance of ferrimagnetic order.<sup>25–27</sup> Since such superexchange interactions are mediated by an intervening oxygen ion, exchange bonds are broken if an oxygen is missing from the surface. In consequence, electrons can no longer participate in the superexchange. This fact is important as far as changes in the electric field gradient on the surface can arise. In principle, this can lead to anisotropy which in turn can be either perpendicular or parallel to the surface, depending on the sign of the crystal-field interaction. On the other hand, surface modification, such as the chemical one, can also induce changes in the surface anisotropy and exchange bias properties, as it has been observed in organic-coated  $\text{NiFe}_2\text{O}_4$  particles.<sup>11,13,14</sup> In particular, magnetite nanoparticles with a chemically modified surface have also been successfully synthesized. An important recent effort in that direction to understand the effect of surfactant coating on the magnetic properties of  $\text{Fe}_3\text{O}_4$  nanoparticles, by means of electronic spin resonance (ESR), has been made by Koseoglu.<sup>28</sup> In that work, nanoparticles were coated with gold, Na-oleate and methoxypolyethylene glycol. Results showed remarkable differences in the resonance fields and line width of the ESR spectra, indicating strong magnetic surface effects depending on the coating medium. In the same direction, other related works demonstrating the influence of the coating medium on the magnetic properties of magnetite nanoparticles have also been recently addressed.<sup>29–31</sup> Hence, it is clear that the matrix where particles can be embedded, the surfactant, the coating medium surrounding the surface of the particles, or even the specific way by which the particle surface ends at atomic level, act as important sources of surface anisotropy.

Magnetite has recently been of particular interest for being an excellent candidate for spintronics applications due to the high degree of spin polarization in one of the spin subbands at the Fermi level and at room temperature.<sup>32–35</sup> Different facts point out to the surface of magnetite at nanoscale

behaving in an entirely different manner than bulk magnetite. Surface studies in magnetite thin films showed the influence of surface morphology, roughness, and stoichiometric inhomogeneities on the electronic structure.<sup>36</sup> *Ab initio* calculations by employing density functional theory (DFT) with the generalized gradient approximation (GGA) and local-density approximation+ $U$  approaches to determine the electronic structure for five different (111) surfaces of  $\text{Fe}_3\text{O}_4$  revealed that, depending on the particular cation distribution on the surface, either metallic or half-metallic (as in bulk  $\text{Fe}_3\text{O}_4$ ) behavior can be found.<sup>33</sup> A half-metal to metal transition at the (100)  $\text{Fe}_3\text{O}_4$  surface has been also observed by means of spin-resolved photoemission experiments on epitaxial and high quality thin films as well as by DFT-GGA calculations.<sup>37</sup> Such a half-metal to metal transition has also been confirmed by using first-principles calculations in four different  $\text{Fe}_3\text{O}_4$  (001) surfaces.<sup>38</sup>

Different theoretical models and numerical approaches, including recent experimental findings,<sup>20</sup> have also been performed in order to contribute to the current understanding of exchange bias in nanoparticles.<sup>39–45</sup> Despite all the important amount of papers on this direction, to our knowledge, the effect of the surface anisotropy constant, as a driving force for giving rise to exchange bias in pure ferrimagnetic nanoparticles, has not yet been explored. In this work we present a Monte Carlo study, based on a classical Heisenberg model, to address the effect of surface anisotropy on the exchange bias behavior in magnetite nanoparticles. The layout of the paper is as follows. In Sec. II we introduce the model, the Hamiltonian, describing the interactions to be considered, simulation details, and the observables to be computed. Numerical results and discussions are presented in Sec. III. This section shows (i) the hysteretic properties for different particle diameters and for two different surface anisotropy scenarios, (ii) the effect of strong surface anisotropy upon the hysteretic and exchange bias properties at low temperatures for nanoparticles of 2.5 nm in diameter, and finally (iii) the temperature dependence of the coercive force and susceptibility for two different surface anisotropy values and nanoparticles of 2.5 nm in diameter. Conclusions are finally presented in Sec. IV.

## II. MODEL AND MONTE CARLO SIMULATION

The model employed in this study reproduces the inverse spinel crystalline structure of magnetite ( $\text{Fe}_3\text{O}_4$ ) with symmetry  $Fd\bar{3}m$ . In this cubic structure a total number of 56 ions per unit cell are considered. They are distributed as follows: 32  $\text{O}^{2-}$  oxygen ions, 8  $\text{Fe}^{3+}$  iron ions in tetrahedral sites ( $A$ -sites), and finally 8  $\text{Fe}^{2+}$  and 8  $\text{Fe}^{3+}$  ions randomly located in octahedral sites ( $B$ -sites). Those iron cations belonging to  $B$ -sites are responsible for the nonresolved sextet observed by Mössbauer spectroscopy above the Verwey temperature. Such sextet corresponds to the  $\text{Fe}^{2.5+}$  mixed valence state resulting from an electron hopping mechanism between  $\text{Fe}^{2+}$  and  $\text{Fe}^{3+}$  cations.<sup>46</sup> The corresponding chemical formula can be written as

$$(\text{Fe}^{3+})_A[\text{Fe}^{2+}\text{Fe}^{3+}]_B\text{O}_4^{2-}. \quad (1)$$

Magnetic moments of iron cations were represented by classical Heisenberg spins. Their magnitudes have been considered taking into account their respective valence states and therefore their corresponding electronic configurations, namely,  $[\text{Ar}]3d^5$  for  $\text{Fe}^{3+}$  and  $[\text{Ar}]3d^6$  for  $\text{Fe}^{2+}$ . Thus, a value of  $S=5/2$  was used for  $\text{Fe}^{3+}$  and  $S=2$  for  $\text{Fe}^{2+}$ . Oxygen ions, which mediate in the superexchange interactions, were considered as nonmagnetic. Spins interact via AFM couplings when considering the following bonds:  $\text{Fe}_A^{3+}-\text{Fe}_A^{3+}$ ,  $\text{Fe}_A^{3+}-\text{Fe}_B^{3+}$ , and  $\text{Fe}_A^{3+}-\text{Fe}_B^{2+}$ . By contrast, the following couplings were considered FM:  $\text{Fe}_B^{3+}-\text{Fe}_B^{3+}$ ,  $\text{Fe}_B^{3+}-\text{Fe}_B^{2+}$ , and  $\text{Fe}_B^{2+}-\text{Fe}_B^{2+}$ . Numerical values of the integrals employed were  $J_{AA}=-0.11$  meV,  $J_{BB}=+0.63$  meV, and  $J_{AB}=-2.92$  meV.<sup>25</sup> Hence, the sign and greater magnitude of the intersublattice integral  $J_{AB}$  accounts for antiparallel intersublattice alignment. This fact, in addition to the different spin values, explains the ferrimagnetic behavior observed in bulk magnetite below the Curie temperature. The classical Heisenberg Hamiltonian describing our system can be written as follows:

$$\begin{aligned} \mathcal{H} = & -2 \sum_{\langle i,j \rangle} J_{ij} \mathbf{S}_i \cdot \mathbf{S}_j - K_V \sum_i (S_{x,i}^2 S_{y,i}^2 + S_{y,i}^2 S_{z,i}^2 + S_{x,i}^2 S_{z,i}^2) \\ & - K_S \sum_k (S_k \mathbf{e}_k)^2 - g \mu_B \mathbf{H} \cdot \sum_i \mathbf{S}_i. \end{aligned} \quad (2)$$

The first sum involves nearest magnetic neighbors interactions. The number of terms in this sum depends on the coordination numbers. Under bulk conditions three different coordination numbers are identified:  $z_{AA}=4$ ,  $z_{BB}=z_{BA}=6$ , and  $z_{AB}=12$ . These numbers apply for the core, whereas the surface is defined as formed by iron ions having coordination numbers smaller than those corresponding to bulk conditions. The second term in Eq. (2) is the core cubic magneto-crystalline anisotropy and  $K_V$  ( $=0.002$  meV/spin) is the first-order bulk anisotropy constant.<sup>47</sup> The third term accounts for the single-ion site surface anisotropy where the unitary vector  $\mathbf{e}_k$  is computed on every  $k$ th position taking into account the positions  $\mathbf{P}_j$  of the nearest magnetic neighbors.<sup>48</sup>

$$\mathbf{e}_k = \frac{\sum_j (\mathbf{P}_k - \mathbf{P}_j)}{\left| \sum_j (\mathbf{P}_k - \mathbf{P}_j) \right|}. \quad (3)$$

Positions over which these vectors were computed correspond exclusively to Fe-cations on the surface. The last term in Eq. (2) gives the interaction of spins with a uniform external magnetic field. Estimates of the different energies involved, including dipole-dipole interactions over the entire volume, were initially performed. Such estimates yielded the following orders of magnitude:  $\sim 10^3$  meV/spin for superexchange interactions,  $\sim 10^{-2}$  meV/spin for surface anisotropy,  $\sim 10^{-4}$  meV/spin for cubic anisotropy, and  $\sim 10^{-5}$  meV/spin for dipole-dipole interactions. Therefore, dipolar interactions were neglected in the present study.<sup>49</sup> Regarding the Monte Carlo simulation, we have employed a single-spin movement Metropolis dynamics. Averages were computed over 25 different samples corresponding to five

different magnetic starting configurations and five different realizations of  $\text{Fe}^{3+}$  and  $\text{Fe}^{2+}$  ions at octahedral sites per each initial magnetic configuration. Hence, error bars were computed. A maximum number of  $5 \times 10^5$  Monte Carlo steps per spin (MCS) were used and the first  $2 \times 10^5$  steps were discarded for equilibration. The lowest temperature considered was 10 K and no special considerations on crystalline symmetry were made for temperatures below the Verwey temperature  $T_V$  known to be at around 120 K for bulk magnetite. The reason for this is experimentally endorsed by several studies in which the suppression of the Verwey transition takes place for particle sizes below 20 nm.<sup>47,50,51</sup> We want to stress however that investigations on magnetite nanoparticles with monoclinic symmetry are currently under progress. Numerical values for the  $K_S/K_V$  ratio were taken to range between 1 and  $10^4$ . Such extreme values allow: (i) to determine the stability of the magnetic structures involved and (ii) to model different experimental and likely scenarios where a given matrix or coating medium, such as an organic surfactant, can effectively change the surface anisotropy. Some few simulation studies addressing the effect of strong surface anisotropy can be found in the literature.<sup>49,52-61</sup> Nearly spherical nanoparticles of different diameters were considered:  $D=2, 2.5, 3.0, 3.5, 4, 4.5, 5, 6,$  and  $7$  nm. Free boundary conditions were implemented and the thermodynamic quantities computed were the energy, the magnetization per spin, the magnetic susceptibility, and the specific heat. Contributions to the total magnetization, magnetic susceptibility, and hysteresis loops, arising from  $A$  and  $B$  sites, as well as from core and surface, were separately computed.

### III. RESULTS AND DISCUSSION

#### A. Hysteresis loops for low surface anisotropy

In order to study the effect of particle size on the hysteresis properties temperature was set to 10 K and  $K_S/K_V=10$ . Hysteresis loops for different particle diameters are shown in Fig. 1. Cycles are characterized by a high degree of squareness, associated with the reversal of the magnetization as a whole, and a marked tendency of the saturation magnetization and the remanence to decrease as the particle size decreases. Under bulk conditions the saturation magnetization per spin goes to  $2/3$  accordingly with stoichiometry and the different Fe spin values involved. Values close to this limit were obtained for nanoparticles of 6 and 7 nm in diameter, whereas finite size effects become evident for smaller nanoparticles having smaller values of the saturation magnetization per spin. Here, magnetization reduction is due to uncompensated spins on the surface and not to a surface spin canting phenomenology. Moreover, in the remanence and the saturation states magnetic structure is characterized by an almost perfect ferrimagnetic alignment of the spins in the entire volume of the nanoparticle for the considered surface anisotropy value (Fig. 2).

By plotting separately the core and surface contributions to the total magnetization, as shown in Fig. 3, for a given particle size, both the loops of the core and the surface are almost square. This result holds independently of the particle size for  $K_S/K_V=10$ . This result implies a reversal of the mag-

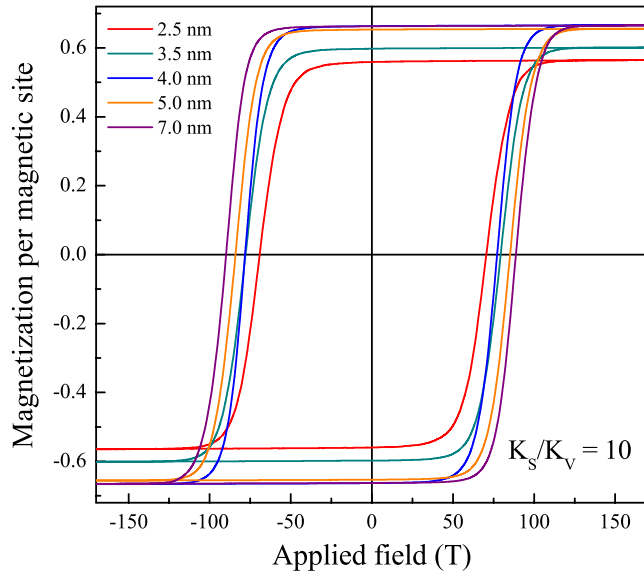


FIG. 1. (Color online) Hysteresis loops at 10 K and  $K_S/K_V=10$  for different particle sizes. Both coercive force and remanence tend to diminish as the particle size decreases.

netization as a whole with a well-defined ferrimagnetic moment, i.e., nanoparticles behave like macrospins, as in the Stoner–Wohlfarth model.<sup>49</sup> Additionally, it is the reversal of the surface spins which triggers the reversal of the core. This is indicated by the fact that the switching field of the surface is slightly smaller to the one of the core (open circles in Fig. 3). Concerning exchange bias properties at these low  $K_S$  values, no shifted loops can be confirmed within the degree of precision provided by the error bars.

As the surface anisotropy increases hysteresis loops become substantially different. Figure 4 shows the hysteresis loops for different particle diameters at  $T=10$  K and  $K_S/K_V=3000$ . In this case, hysteresis loops remain symmetric but different from those cycles at smaller surface anisotropy values, hysteresis loops now appear less square and more elongated. Remanence reduction becomes now more remarkable as the particle size decreases. This fact is mainly

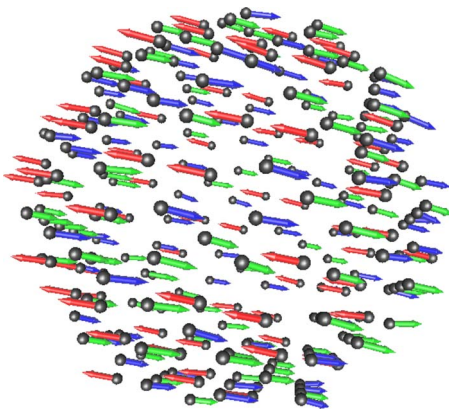


FIG. 2. (Color online) Surface magnetic structure for a nanoparticle of 3 nm at 10 K and  $K_S/K_V=10$ . Ferrimagnetic alignment is preserved both on the surface and in the core. Arrows represent Fe spins: gray (red) color for  $\text{Fe}_A^{3+}$  ions (pointing to the left), dark gray (blue) for  $\text{Fe}_B^{3+}$  ions, and light gray (green) for  $\text{Fe}_B^{2+}$  (both of them pointing to the right).

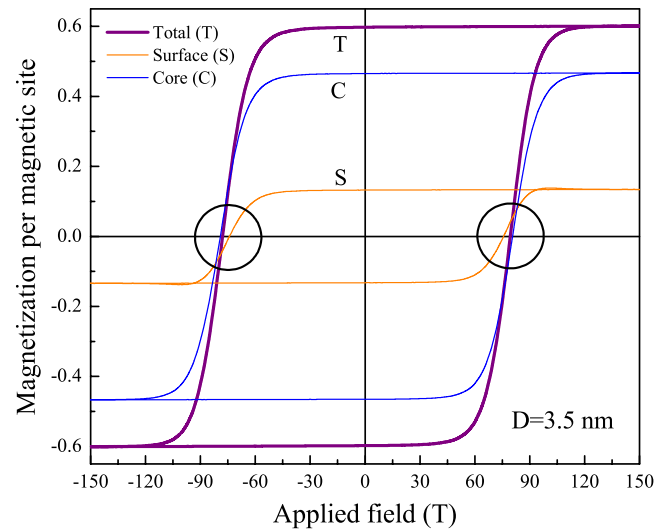


FIG. 3. (Color online) Total ( $T$ ), surface ( $S$ ), and core ( $C$ ) contributions to the hysteresis loop for  $D=3.5$  nm at  $T=10$  K and  $K_S/K_V=10$ . Similar results were obtained for all the particle sizes. Coercive force of the surface is slightly smaller than that of the core (open circles).

due to a small tendency of the surface spins to be pinned along radial directions for which magnetic structures are of the throttled type.<sup>55,58</sup>

Figure 5 shows the variation with the particle diameter of the coercive force for the two surface anisotropy values above considered. As can be observed, coercivity displays an increasing monotonic size dependence whose slope changes depending on the surface anisotropy. For  $K_S/K_V=3000$  the switching field follows the same increasing behavior as the particle size increases, but now the obtained values are greater by keeping the same conditions than those obtained for  $K_S/K_V=10$ . The reason for that is the increase, via  $K_S$ , in the height of the energy barrier to be overcome. Even though the reversal of magnetization can be considered coherent, deviations from the number of core spins relative to the total ( $N_c/N$ ) are observed. This means that only those particles

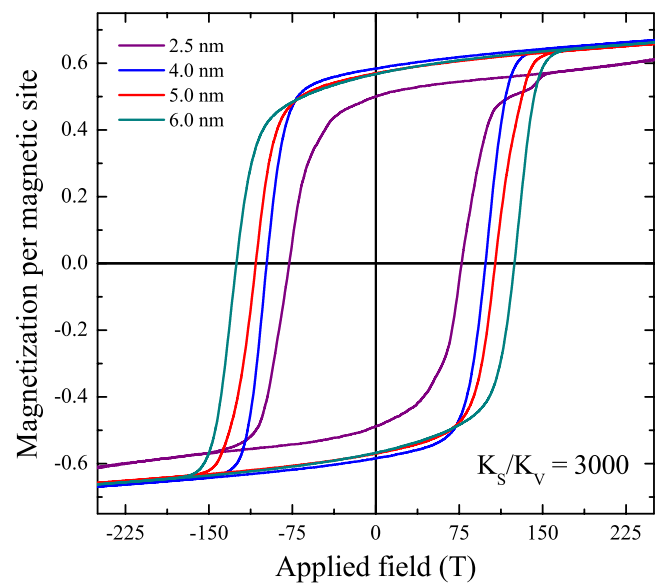


FIG. 4. (Color online) Hysteresis loops at 10 K and  $K_S/K_V=3000$  for different particle sizes. Coercive force diminishes as the particle size decreases.

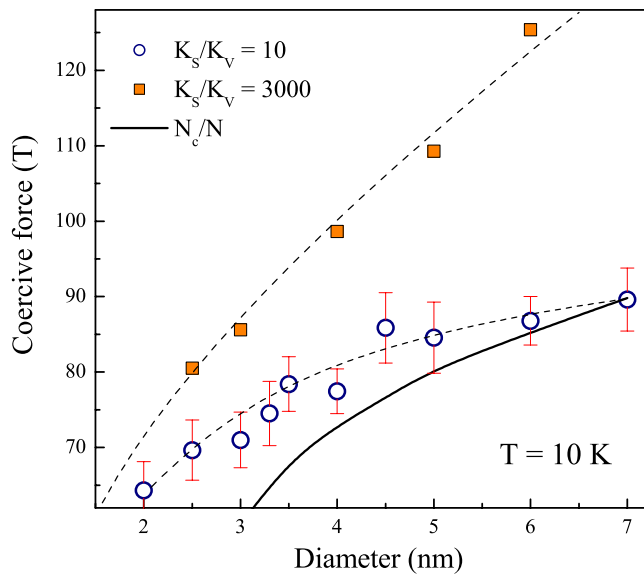


FIG. 5. (Color online) Low temperature coercive force as a function of the particle diameter for two different  $K_S/K_V$  ratios. Dashed lines are guides to the eyes.

with small surface anisotropy and bigger size behave accordingly with the Stoner–Wohlfarth model.<sup>49</sup> As the particle size is reduced the density of magnetic bonds decreases as long as the proportion of undercoordinated ions on the surface becomes greater. Thus, smaller fields enable more easily the reversal of spins and lead to lower switching fields for smaller sizes.

In order to evaluate separately the core and surface behaviors regarding the hysteretic properties for  $K_S/K_V=3000$ , Fig. 6 shows the core and surface contributions to the hysteresis loops for a 2.5 nm nanoparticle and  $K_S/K_V=3000$ . Results indicate a progressive reversal of the surface magnetization which is a typical feature associated with disordered or frustrated systems. Analogously to what was observed for

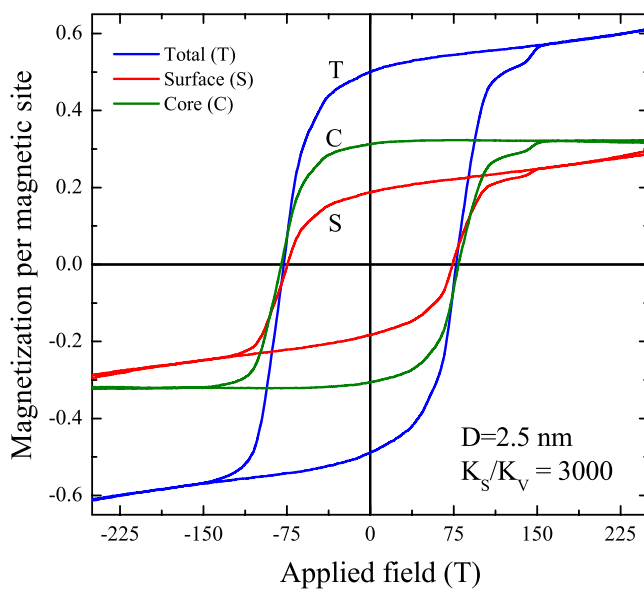


FIG. 6. (Color online) Total ( $T$ ), surface ( $S$ ), and core ( $C$ ) contributions to the hysteresis loop for  $D=2.5$  nm at  $T=10$  K and  $K_S/K_V=3000$ .

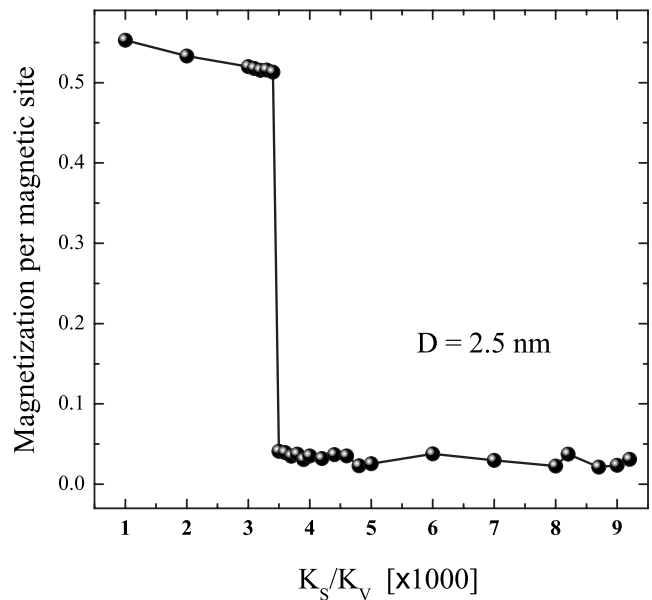


FIG. 7. Dependence of the magnetization with the  $K_S/K_V$  ratio at  $T=10$  K for nanoparticles of  $D=2.5$  nm.

$K_S/K_V=10$ , the reversal of the surface spins triggers the reversal of the core, and the core magnetization tends to be reversed as a whole besides being saturable.

It must be stressed that most of the zero-field magnetic structures for the range of values of  $K_S/K_V$  considered up to here are characterized for having a well-defined ferrimagnetic alignment along the (111) direction for  $K_S/K_V=10$  (Fig. 2), whereas for  $K_S/K_V=3000$  the magnetic structure is of the throttled type<sup>55,58</sup> where it is more noticeable the tendency of surface spins to be perpendicular to the surface. For greater surface anisotropy values beyond certain threshold, which depends on the system size, magnetic structures become of the hedgehog type with magnetization close to zero. Figure 7 shows the dependence of the zero-field magnetization with the surface anisotropy over a wide range of values for nanoparticles of 2.5 nm in diameter. A  $K_S$ -driven magnetic transition is observed, where for values above  $K_S/K_V \approx 3500$  the magnetic structure is of the hedgehog type, as that shown in Fig. 8.

## B. Hysteresis loops for high surface anisotropy

Concerning exchange bias properties, shifted loops were evidenced for nanoparticles having some specific ranges of high enough surface anisotropy values above  $K_S/K_V=3000$ , as can be observed in Fig. 9, for a nanoparticle of 2.5 nm. Exchange bias can be understood in terms of the different paths followed by the core and surface spins during the reversal process of the magnetization. High values of the surface anisotropy constant make the surface spins to be pinned and consequently the surface becomes magnetically hard during the reversal process. This is the reason for the progressive reversal of the surface magnetization and the high degree of irreversibility upon cycling the applied field. Contrary to this, the core of the nanoparticle, where the anisotropy remains fixed and much smaller than that of the surface, behaves in a softer manner. Such a hard-soft interplay

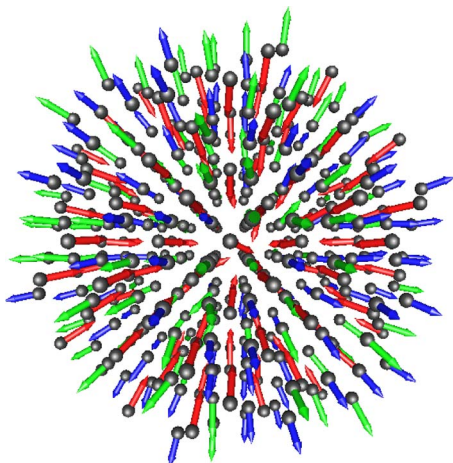


FIG. 8. (Color online) Magnetic structure for a nanoparticle of  $D=3$  nm at  $T=10$  K and  $K_S/K_V=7000$ . Arrows represent Fe spins: gray (red) color for  $\text{Fe}_A^{3+}$  ions (inwards), dark gray (blue) for  $\text{Fe}_B^{3+}$  ions, and light gray (green) for  $\text{Fe}_B^{2+}$  (both of them outwards).

between surface and core gives rise to the occurrence of an interface across which surface and core spins interact via superexchange couplings. On the other hand, uncompensated spins on the surface, where different spin values are involved, are not necessarily symmetrically distributed due to the finiteness and discreteness of the system. This fact is more evident for smaller nanoparticles. Such spins, strongly pinned, tend to exert a microscopic torque on the core spins. Once the field is applied some of those torques become favored, depending on the direction along which the field is applied. As a result, and due to the nonsymmetric distribution of such torques, a hysteresis loop shift, which can be positive or negative, will be observed along the field axis. Similar mechanisms for explaining exchange bias properties have been also suggested to occur in oxide-coated manganese nanoparticles.<sup>57</sup> The evidence for the occurrence of such torques has been already demonstrated in previous studies at

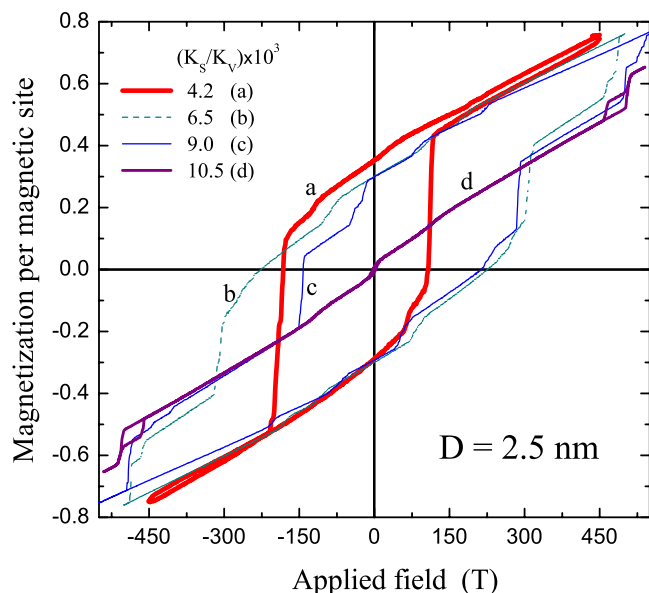


FIG. 9. (Color online) Hysteresis loops for nanoparticles of  $D=2.5$  nm at  $T=10$  K and different  $K_S/K_V$  values.

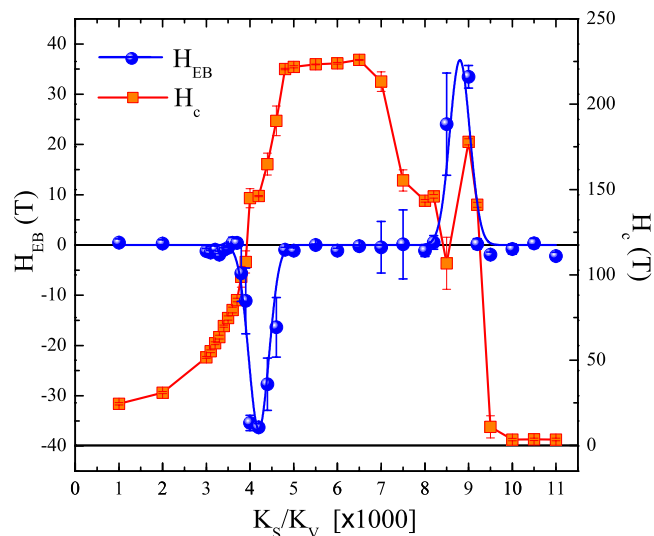


FIG. 10. (Color online) Dependence of both the exchange bias and coercive force with the surface anisotropy for nanoparticles of 2.5 nm in diameter and  $T=10$  K.

zero field, where the tendency of the surface spins to be radially oriented is propagated through the core via superexchange couplings giving rise to hedgehog-type magnetic states, as that shown in Fig. 8.<sup>55,57,58</sup> Summarizing, the tendency of the surface spins to be more or less compensated, depending on the particle size, in addition to the different ratio of octahedral to tetrahedral spins,<sup>62</sup> explains why the values of surface anisotropy for which exchange bias appears, and it can be positive or negative, are different for different system sizes.

Figure 10 shows both the dependence of exchange bias and coercive force as a function of  $K_S/K_V$ . As can be observed, for intermediate values of the ratio  $K_S/K_V$  around 4200, a negative exchange bias is observed, whereas for higher values of this ratio around 9000 exchange bias becomes positive.

Such a particular scenario can be understood by analyzing the different contributions to the total magnetization in the hysteresis loops as can be observed in Figs. 11–13 for three different  $K_S/K_V$  values. At around  $K_S/K_V \approx 4200$ , once the magnetization of octahedral sites, which is the major contribution to the total magnetization, is reversed when passing from point c to d in Fig. 11, some of the  $\text{Fe}_B$  spins remain pinned and relatively unaffected with a projection along the field axis opposite to the field direction. Such spins store energy like a torsion spring and they exert an additional torque on the reversible spins. This fact implies that the following magnetization reversal, from point g to h, takes place at lower fields resulting in a negative exchange bias. This can be concluded because the magnitude of the magnetization in the positive field direction is larger than that in the opposite direction, which indicates that some of the spins are pinned in the positive field direction and cannot be reversed by the field. The difference between these two magnetizations is proportional to the number of pinned spins. Moreover, the zero-field magnetization (remanence) at point b is greater in magnitude than that at point f where the unreversed spins make the absolute value of the magnetization be smaller re-

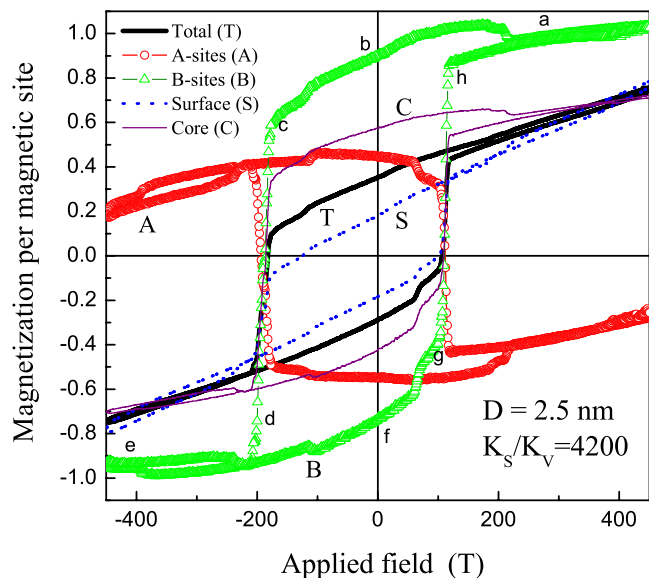


FIG. 11. (Color online) Total ( $T$ ), surface ( $S$ ), core ( $C$ ), tetrahedral ( $A$ ), and octahedral ( $B$ ) contributions to the hysteresis loops for  $D=2.5$  nm,  $T=10$  K, and  $K_S/K_V=4.2 \times 10^3$ .

sulting in turn in an upwards magnetization vertical shift. Concurrently, the contribution to the hysteresis loops from  $Fe_A$  spins undergoes a downwards vertical shift as a consequence of the intersublattice AFM coupling, which is larger than the intrasublattice coupling. As the surface anisotropy increases, the tendency of the surface spins to be perpendicular to the surface begins to propagate to the core via superexchange couplings. This fact makes the overall system magnetically harder and consequently the coercive force increases. At this stage the gradual reversal of the magnetization is complete, i.e., there are not unreversed spins, giving rise to a symmetry at both negative and positive fields, and therefore no exchange bias is observed (Fig. 12). As we go further in the value of surface anisotropy at around  $K_S/K_V$

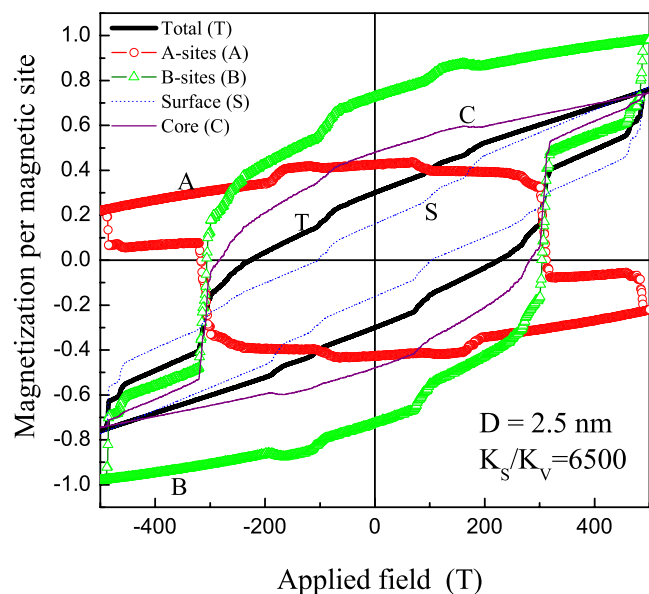


FIG. 12. (Color online) Total ( $T$ ), surface ( $S$ ), core ( $C$ ), tetrahedral ( $A$ ), and octahedral ( $B$ ) contributions to the hysteresis loops for  $D=2.5$  nm,  $T=10$  K, and  $K_S/K_V=6.5 \times 10^3$ .

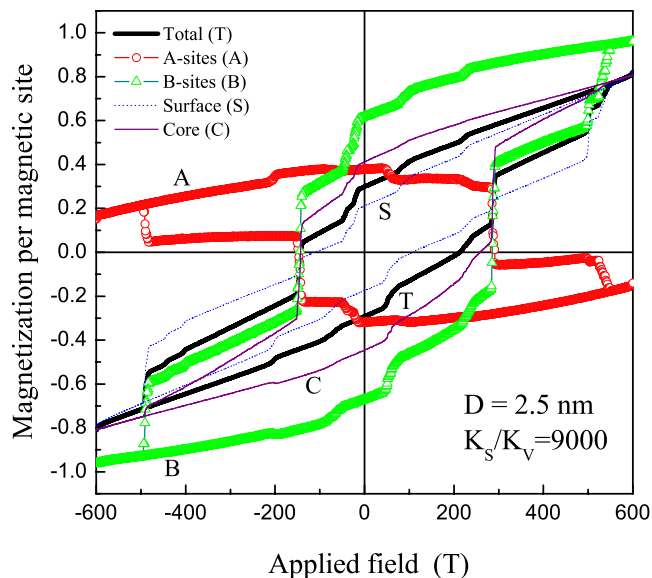


FIG. 13. (Color online) Total ( $T$ ), surface ( $S$ ), core ( $C$ ), tetrahedral ( $A$ ), and octahedral ( $B$ ) contributions to the hysteresis loops for  $D=2.5$  nm,  $T=10$  K, and  $K_S/K_V=9 \times 10^3$ .

$\approx 9000$ , a downwards vertical shift in the  $Fe_B$  spins cycle appears, giving rise to a positive exchange bias (Fig. 13). This fact can be understood as due to the interplay between the Zeemann energy and the surface anisotropy for which the amount of unreversed spins increases again. Differently from the earlier stage at lower  $K_S/K_V$  values, more unreversed spins are aligned or closely aligned opposite to the positive field direction, and those spins with anisotropy axis perpendicular or closely perpendicular to the field axis are forced to follow the field direction. Once the field is reversed, those spins pinned along the negative field direction exert an additional torque on the reversible  $Fe_B$  spins resulting in a positive exchange bias. Cycles reveal also that nucleation begins before switching the field in correspondence with a high degree of irreversibility. This behavior differs from that observed at low  $K_S/K_V$  values below 3000, where the symmetry in the magnetization values both at positive and negative fields indicates the absence of pinned spins (Fig. 1). It must be stressed at this point that the distribution of pinned spins is not symmetric. Finally, for huge values of  $K_S/K_V$  above 9000, the hedgehog-type magnetic structure becomes practically rigid giving rise to the absence of both coercivity and exchange bias (Fig. 10). Hysteresis loops are characterized by steps or jumps, which become more pronounced as the surface anisotropy increases. Such jumps are attributed to the high degree of spin pinning, for which reversal does not occur in a continuous fashion, and to a discrete shift in the center of symmetry of the magnetic moment distribution in the direction opposite to the field.<sup>55</sup> As is well established, in order to generate exchange bias it is necessary to have the presence of at least two exchange-coupled phases: a reversible phase whose magnetic moments can be reversed and a fixed phase whose moments cannot be reversed. In our case those pinned spins, which belong to the surface or even to the core, play the role of the fixed phase. On the other hand, the reversible phase includes both the contributions of the

core and the reversible part of the surface. The relative proportion of each phase will depend on the magnitude of the surface anisotropy. Summarizing, exchange bias results from the coupling between the pinned spins, strongly influenced by the surface anisotropy, and the reversible spins. Experimentally, vertical shifts have been recently reported to occur in similar systems to the one considered here such as  $\text{CoFe}_2\text{O}_4$  nanoparticles.<sup>63</sup> Here, vertical shifts, accompanying the exchange bias, were associated with the presence of strongly pinned uncompensated spins at the core-shell interface. Analogously, frozen spins in  $\gamma\text{-Fe}_2\text{O}_3$  coated Fe nanoparticles are responsible for both horizontal and vertical shifts in the hysteresis loops.<sup>64</sup> In this last case, it is a spin-glasslike phase with high-field irreversibility in the  $\gamma\text{-Fe}_2\text{O}_3$  shell that plays the role of the fixed phase. Large shifts in both horizontal and vertical directions have also been found in milled  $\text{Fe}/\text{MnO}_2$  systems<sup>65</sup> having some similarities to the one studied here where shifts were attributed to a large surface contribution of a noncollinear magnetic structure.

In short, as the surface anisotropy increases the magnetization reversal process becomes progressively gradual. For  $K_S/K_V$  ratios above certain threshold value of approximately  $5 \times 10^3$ , several features are remarkable: (i) cycles are widely elongated and open up to approximately the maximum applied field, (ii) magnetization reversal occurs step by step, suggesting a distribution of switching fields or rotational barriers, (iii) it is the reversal of the surface spins which triggers the reversal of the core, and (iv) exchange bias properties appear. Once the field is applied on a hedgehog-type nanoparticle, very high fields are required to force transitions between surface spins and to overcome the high degree of pinning of the magnetic moments. This fact explains the high-field irreversibility. In literature some results have been reported for  $\text{NiFe}_2\text{O}_4$  nanoparticles showing the persistence of hysteresis up to 16 T, 400 times larger than the bulk magnetocrystalline anisotropy field.<sup>13</sup> Exchange bias and the presence of jumps during magnetization reversal are also attributed to the high degree of surface spin pinning. In our case, surface spin pinning is relevant at high enough surface anisotropy values above the threshold when such behavior tends to propagate through the core via superexchange couplings.

### C. Thermal Effects

Figure 14 shows the temperature dependence of the coercivity for two different  $K_S/K_V$  ratios and  $D=2.5$  nm. Coercivity decreases with increasing temperature and vanishes at around 450 K. Contrary to this, exchange bias remains almost zero (within the error bars).

Another important feature that allows us to understand the already mentioned hard-soft interplay between surface and core is illustrated finally in Figs. 15 and 16. These figures show the surface and core contributions to the total magnetic susceptibility as a function of temperature for a nanoparticle of  $D=2.5$  nm, two different  $K_S/K_V$  ratios, and zero field. The fact that the temperature at which the surface susceptibility reaches the maximum is lower than that found at the core indicates that both surface and core behave in a

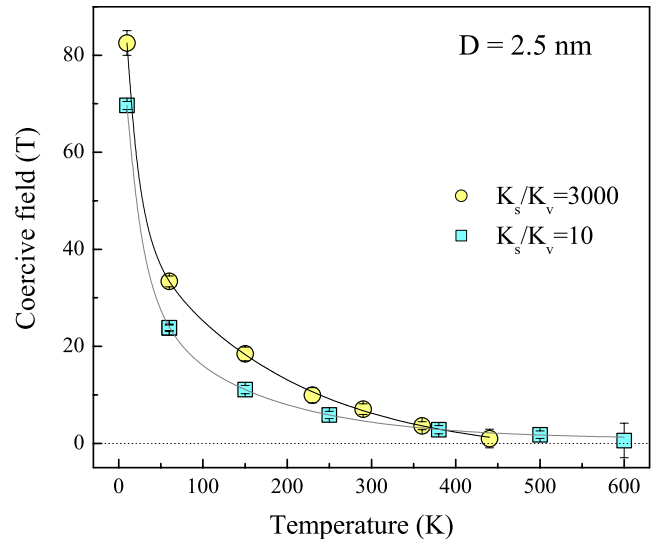


FIG. 14. (Color online) Temperature dependence of the coercivity for two different  $K_S/K_V$  ratios and  $D=2.5$  nm.

different manner. This phenomenology resembles a phase separation process and suggests that the phase transition takes place in a very gradual fashion. In the case of very high anisotropy values (see Fig. 16), results reveal a marked tendency to diverge in a very narrow range of temperature. This feature is attributed to the sharp transition to the hedgehog structure characterized by a magnetization close to zero in the low temperature regime.

Finally, we want to comment that coercive force values obtained through simulation cannot be directly compared to those experimentally reported. As is well established experimentally as well as numerically, the coercivity depends on the speed at which the applied field is varied. In Monte Carlo simulations that speed is determined by the number of Monte Carlo steps employed in computing the ensemble averages and the field step size during the cycle. That means that, in principle, it is possible to tune the number of MCS and field step size in order to obtain values similar to those experi-

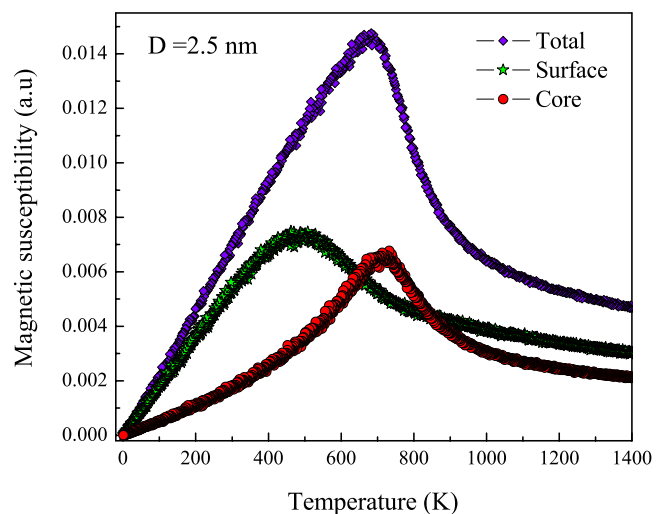


FIG. 15. (Color online) Temperature dependence of the total susceptibility, core and surface contributions for nanoparticles of 2.5 nm in diameter and  $K_S/K_V=10$ .

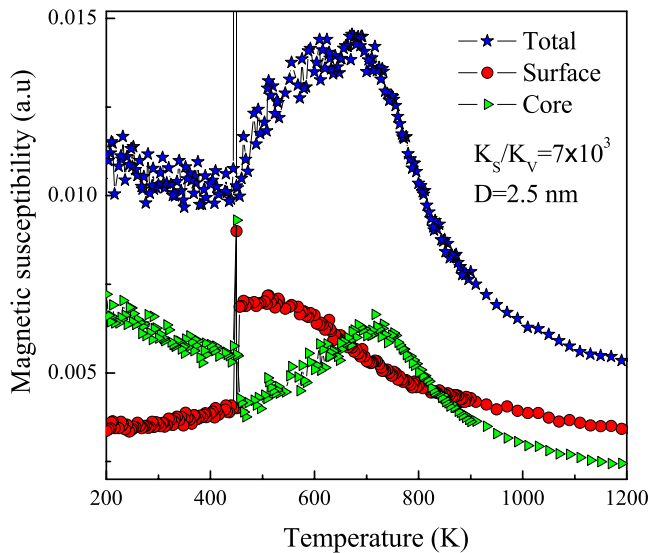


FIG. 16. (Color online) Temperature dependence of the total susceptibility, core and surface contributions for nanoparticles of 2.5 nm in diameter and  $K_S/K_V=7000$ .

mentally achievable, but that demands a huge computational effort. Similar values for the field range have been, for instance, reported elsewhere.<sup>55</sup> However, we want to stress that the conditions (MCS and field step) under which our hysteresis loops were recorded remained fixed in all the cases, which allows comparison among them. Comparisons with experiment are also difficult as far as hysteresis loops for an isolated magnetite nanoparticle have to date not been reported, and those found in the literature correspond to assemblies of interacting nanoparticles.<sup>47</sup>

#### IV. CONCLUSIONS

The effect of surface anisotropy and particle size on the hysteretic and magnetic properties of magnetite nanoparticles has been addressed. Results revealed that the magnitude of the surface anisotropy constant can act as a driving force giving rise to the occurrence of a strong surface spin pinning. Exchange bias behavior, which can be positive, negative, or even a vanishing value depending on the particle size, can be attributed to the tendency of the surface spins to be more or less compensated and to the different ratio of octahedral to tetrahedral spins. The pinning mechanism is also the one responsible for magnetization and remanence reduction. Moreover, nanoparticles with a giant surface anisotropy can exhibit, at zero field, spin structures of the hedgehog type characterized by a magnetization close to zero in the low temperature regime. Finally, the differentiated analysis of the core and surface contributions to the total susceptibility allows us to conclude that both regions behave in a different manner resembling a magnetic phase separation process of the hard-soft type, and giving rise to a gradual transition from the ferrimagnetic to the paramagnetic state. More specifically, susceptibility data suggest a magnetically harder character for the surface relative to the core as the surface anisotropy increases. Such a coupled hard-soft interplay is the proposed mechanism for explaining the onset of exchange bias behavior.

#### ACKNOWLEDGMENTS

This study was supported by the Sostenibilidad projects of the GES and GICM groups and the CODI Project No. IN565CE at the Universidad de Antioquia, FONDECYT Grant Nos. 1050066 and 7080111, and the “Millenium Science Nucleus, Basic and Applied Magnetism Grant No. P06-022F” project. One of the authors (J.M.Z) wishes to thank Universidad de Antioquia and COLCIENCIAS for their support.

- <sup>1</sup>W. H. Meiklejohn and C. P. Bean, *Phys. Rev.* **102**, 1413 (1956); **105**, 904 (1957).
- <sup>2</sup>J. Nogués and I. K. Schuller, *J. Magn. Magn. Mater.* **192**, 203 (1999).
- <sup>3</sup>J. Nogués, J. Sort, V. Langlais, V. Skumryev, S. Suriñach, J. S. Muñoz, and M. D. Baró, *Phys. Rep.* **422**, 65 (2005).
- <sup>4</sup>P. J. Van der Zaag, R. M. Wolf, A. R. Ball, C. Bordel, L. F. Feiner, and R. Jungblut, *J. Magn. Magn. Mater.* **148**, 346 (1995).
- <sup>5</sup>W. C. Cain and M. H. Kryder, *J. Appl. Phys.* **67**, 5722 (1990).
- <sup>6</sup>M. Spasova, U. Wiedwald, M. Farle, T. Radetic, U. Dahmen, M. Hilgendorff, and M. Giersig, *J. Magn. Magn. Mater.* **272–276**, 1508 (2004).
- <sup>7</sup>D. S. Geoghegan, P. G. McCormick, and R. Street, *Mater. Sci. Forum* **179–181**, 629 (1995).
- <sup>8</sup>W. H. Meiklejohn, *J. Appl. Phys.* **29**, 454 (1958).
- <sup>9</sup>V. Papaefthymiou, A. Kostikas, A. Simopoulos, D. Niarchos, S. Gangopadhyay, G. C. Hadjipanayis, C. M. Sorensen, and K. J. Klabunde, *J. Appl. Phys.* **67**, 4487 (1990).
- <sup>10</sup>C. M. Hsu, H. M. Lin, and K. R. Tsai, *J. Appl. Phys.* **76**, 4793 (1994).
- <sup>11</sup>R. H. Kodama, A. E. Berkowitz, E. J. McNiff, Jr., and S. Foner, *J. Appl. Phys.* **81**, 5552 (1997).
- <sup>12</sup>R. H. Kodama, S. A. Makhlof, and A. E. Berkowitz, *Phys. Rev. Lett.* **79**, 1393 (1997).
- <sup>13</sup>R. H. Kodama, A. E. Berkowitz, E. J. McNiff, and S. Foner, *Phys. Rev. Lett.* **77**, 394 (1996).
- <sup>14</sup>A. E. Berkowitz, J. A. Lahut, I. S. Jacobs, L. M. Levinson, and D. W. Forester, *Phys. Rev. Lett.* **34**, 594 (1975).
- <sup>15</sup>H. Wang, T. Zhu, K. Zhao, W. N. Wang, C. S. Wang, Y. J. Wang, and W. S. Zhan, *Phys. Rev. B* **70**, 092409 (2004).
- <sup>16</sup>B. Martínez, X. Obradors, L. Balcells, A. Rouanet, and C. Monty, *Phys. Rev. Lett.* **80**, 181 (1998).
- <sup>17</sup>E. Tronc, D. Fiorani, M. Nogués, A. M. Testa, F. Lucari, F. D’Orazio, J. M. Grenèche, W. Wernsdorfer, N. Galvez, C. Chanéac, D. Maily, M. Verdager, and J. P. Jolivet, *J. Magn. Magn. Mater.* **262**, 6 (2003).
- <sup>18</sup>C. Frandsen, C. W. Ostefeld, M. Xu, C. S. Jacobsen, L. Keller, K. Lefmann, and S. Morup, *Phys. Rev. B* **70**, 134416 (2004).
- <sup>19</sup>Ó. Iglesias and A. Labarta, *Physica B* **343**, 286 (2004).
- <sup>20</sup>A. Cabot, A. Paul Alivisatos, V. F. Puentes, L. Balcells, Ó. Iglesias, and A. Labarta, *Phys. Rev. B* **79**, 094419 (2009).
- <sup>21</sup>G. L. Bona, F. Meier, H. C. Siegmann, and R. J. Gambino, *Appl. Phys. Lett.* **52**, 166 (1988).
- <sup>22</sup>E. V. Shipil’, K. Y. Guslienko, and B. Szymanski, *IEEE Trans. Magn.* **30**, 797 (1994).
- <sup>23</sup>N. Sakamoto, *J. Phys. Soc. Jpn.* **17**, 99 (1962).
- <sup>24</sup>Y. Suzuki, R. B. Van Dover, E. M. Gyorgy, J. M. Phillips, V. Korenivski, D. J. Werder, C. H. Chen, R. J. Felder, R. J. Cava, J. J. Krajewski, and W. F. Peck, Jr., *J. Appl. Phys.* **79**, 5923 (1996).
- <sup>25</sup>M. Uhl and B. Siberchicot, *J. Phys.: Condens. Matter* **7**, 4227 (1995).
- <sup>26</sup>P. G. Bercoff and H. R. Bertorello, *J. Magn. Magn. Mater.* **169**, 314 (1997).
- <sup>27</sup>C. M. Srivastava, G. Srinivasan, and N. G. Nanadikar, *Phys. Rev. B* **19**, 499 (1979).
- <sup>28</sup>Y. Koseoglu, *J. Magn. Magn. Mater.* **300**, e327 (2006).
- <sup>29</sup>M. Timko, M. Koneracká, N. Tomasovicová, P. Kocpanský, and V. Závřisová, *J. Magn. Magn. Mater.* **300**, e191 (2006).
- <sup>30</sup>P. Guardia, B. Batlle-Brugal, A. G. Roca, O. Iglesias, M. P. Morales, C. J. Serna, A. Labarta, and X. Batlle, *J. Magn. Magn. Mater.* **316**, e756 (2007).
- <sup>31</sup>A. F. Bakuzis, A. R. Pereira, J. G. Santos, and P. C. Morais, *J. Appl. Phys.* **99**, 08C301 (2006).
- <sup>32</sup>E. Arisi, I. Bergenti, M. Cavallini, M. Murgia, A. Riminucci, G. Ruani, and V. Dediu, *J. Magn. Magn. Mater.* **316**, 410 (2007).
- <sup>33</sup>L. Zhu, K. L. Yao, and Z. L. Liu, *Phys. Rev. B* **74**, 035409 (2006).
- <sup>34</sup>Y. J. Kim, C. Westphal, R. X. Ynzunza, H. C. Galloway, M. B. Salmeron,

- M. A. Van Hove, and C. S. Fadley, *Phys. Rev. B* **55**, R13448 (1997).
- <sup>35</sup>S. K. Park, T. Ishikawa, and Y. Tokura, *Phys. Rev. B* **58**, 3717 (1998).
- <sup>36</sup>K. Jordan, A. Cazacu, G. Manai, S. F. Ceballos, S. Murphy, and I. V. Shvets, *Phys. Rev. B* **74**, 085416 (2006).
- <sup>37</sup>M. Fonin, R. Pentcheva, Yu. S. Dedkov, M. Sperlich, D. V. Vyalikh, M. Scheffler, U. Rüdiger, and G. Güntherodt, *Phys. Rev. B* **72**, 104436 (2005).
- <sup>38</sup>C. Cheng, *Phys. Rev. B* **71**, 052401 (2005).
- <sup>39</sup>Ó. Iglesias, X. Batlle, and A. Labarta, *Phys. Rev. B* **72**, 212401 (2005).
- <sup>40</sup>E. Eftaxias and K. N. Trohidou, *Phys. Rev. B* **71**, 134406 (2005).
- <sup>41</sup>Ó. Iglesias and A. Labarta, *Physica B* **372**, 247 (2006).
- <sup>42</sup>K. N. Trohidou, M. Vasilakaki, L. Del Bianco, D. Fiorani, and A. M. Testa, *J. Magn. Magn. Mater.* **316**, e82 (2007).
- <sup>43</sup>D. Kechrakos, K. N. Trohidou, and M. Vasilakaki, *J. Magn. Magn. Mater.* **316**, e291 (2007).
- <sup>44</sup>Ó. Iglesias, X. Batlle, and A. Labarta, *J. Magn. Magn. Mater.* **316**, 140 (2007).
- <sup>45</sup>M. H. Wu, Q. C. Li, and J.-M. Liu, *J. Phys.: Condens. Matter* **19**, 186202 (2007).
- <sup>46</sup>E. De Grave, R. M. Persoons, R. E. Vandenberghe, and P. M. A. de Bakker, *Phys. Rev. B* **47**, 5881 (1993).
- <sup>47</sup>G. F. Goya, T. S. Berquó, F. C. Fonseca, and M. P. Morales, *J. Appl. Phys.* **94**, 3520 (2003).
- <sup>48</sup>R. H. Kodama and A. E. Berkowitz, *Phys. Rev. B* **59**, 6321 (1999).
- <sup>49</sup>H. Kachkachi and M. Dimian, *Phys. Rev. B* **66**, 174419 (2002).
- <sup>50</sup>J. Wang, Q. Chen, X. Li, L. Shi, Z. Peng, and C. Zeng, *Chem. Phys. Lett.* **390**, 55 (2004).
- <sup>51</sup>N. A. Fellenz, S. G. Marchetti, J. F. Bengoa, R. C. Mercader, and S. J. Stewart, *J. Magn. Magn. Mater.* **300**, 60 (2006).
- <sup>52</sup>D. A. Garanin and H. Kachkachi, *Phys. Rev. Lett.* **90**, 065504 (2003).
- <sup>53</sup>H. Kachkachi and H. Mahboub, *J. Magn. Magn. Mater.* **278**, 334 (2004).
- <sup>54</sup>Ó. Iglesias and A. Labarta, *J. Magn. Magn. Mater.* **272–276**, 685 (2004).
- <sup>55</sup>L. Berger, Y. Labaye, M. Tamine, and J. M. D. Coey, *Phys. Rev. B* **77**, 104431 (2008).
- <sup>56</sup>P. Z. Si, D. Li, J. W. Lee, C. J. Choi, Z. D. Zhang, D. Y. Geng, and E. Brück, *Appl. Phys. Lett.* **87**, 133122 (2005).
- <sup>57</sup>Y. Labaye, O. Crisan, L. Berger, J. M. Greneche, and J. M. D. Coey, *J. Appl. Phys.* **91**, 8715 (2002).
- <sup>58</sup>J. Mazo-Zuluaga, J. Restrepo, and J. Mejía-López, *J. Appl. Phys.* **103**, 113906 (2008).
- <sup>59</sup>J. Mazo-Zuluaga, J. Restrepo, and J. Mejía-López, *Physica B* **398**, 187 (2007).
- <sup>60</sup>J. Restrepo, Y. Labaye, and J. M. Greneche, *Physica B* **384**, 221 (2006).
- <sup>61</sup>J. Restrepo, Y. Labaye, L. Berger, and J. M. Greneche, *J. Magn. Magn. Mater.* **272–276**, 681 (2004).
- <sup>62</sup>J. Mazo-Zuluaga, J. Restrepo, and J. Mejía-López, *J. Phys.: Condens. Matter* **20**, 195213 (2008).
- <sup>63</sup>A. Mumtaz, K. Maaz, B. Janjua, S. K. Hasanain, and M. F. Bertino, *J. Magn. Magn. Mater.* **313**, 266 (2007).
- <sup>64</sup>R. K. Zheng, G. H. Wen, K. K. Fung, and X. X. Zhang, *Phys. Rev. B* **69**, 214431 (2004); *J. Appl. Phys.* **95**, 5244 (2004).
- <sup>65</sup>E. C. Passamani, C. Larica, C. Marques, J. R. Proveti, A. Y. Takeuchi, and F. H. Sánchez, *J. Magn. Magn. Mater.* **299**, 11 (2006).